

**Spin Seebeck effect in Y-type hexagonal ferrite thin films**

J. Hirschner,<sup>1,2</sup> M. Maryško,<sup>1</sup> J. Hejtmánek,<sup>1</sup> R. Uhrecký,<sup>3</sup> M. Soroka,<sup>3</sup> J. Buršík,<sup>3</sup> A. Anadón,<sup>4,5</sup>  
M. H. Aguirre,<sup>4,5</sup> and K. Knížek<sup>1,\*</sup>

<sup>1</sup>*Institute of Physics of the CAS, Cukrovarnická 10, 162 00 Prague 6, Czech Republic*

<sup>2</sup>*Department of Solid State Engineering, Faculty of Nuclear Sciences and Physical Engineering,  
Czech Technical University in Prague, Trojanova 13, 120 00 Prague 2, Czech Republic*

<sup>3</sup>*Institute of Inorganic Chemistry of the CAS, 250 68 Řež, Czech Republic*

<sup>4</sup>*Instituto de Nanociencia de Aragón and Laboratorio de Microscopias Avanzadas, Universidad de Zaragoza, E-50018 Zaragoza, Spain*

<sup>5</sup>*Departamento de Física de la Materia Condensada, Universidad de Zaragoza, E-50009 Zaragoza, Spain*

(Received 6 May 2017; revised manuscript received 19 July 2017; published 23 August 2017)

The longitudinal spin Seebeck effect (SSE) has been investigated using Pt/ferrite bilayers employing two Y-hexagonal ferrites Ba<sub>2</sub>Zn<sub>2</sub>Fe<sub>12</sub>O<sub>22</sub> (Zn2Y) and Ba<sub>2</sub>Co<sub>2</sub>Fe<sub>12</sub>O<sub>22</sub> (Co2Y) deposited by a spin-coating method on SrTiO<sub>3</sub>(111) substrates. The prepared hexagonal ferrites are highly oriented with *c* axes perpendicular to the substrate plane. The room-temperature magnetic moments of both ferrimagnetic ferrites amount to similar values and, most importantly, both have easy magnetization normal to the *c* axis. Despite their similar magnetic response the notable SSE signal is only observed for Zn2Y whereas the SSE signal of Co2Y is below the experimental noise level. A plausible explanation for this surprising discrepancy is magnetic disorder induced by cobalt cations, the random distribution of which in the Co2Y ferrite structure might critically limit the spin-wave propagation. This results in suppression of the SSE signal in Co2Y, while the Zn2Y with nonmagnetic substituent exhibits significant SSE signal. The temperature dependence of SSE for Zn2Y was measured over the 30–300-K range and quantitatively analyzed considering the heat flow through the Pt/Zn2Y bilayer and thermal gradient across the Zn2Y thin layer as the most relevant parameters. Using this approach the normalized SSE smoothly increases with lowering temperature, which correlates to increasing magnon propagation length and magnetization with decreasing temperature.

DOI: [10.1103/PhysRevB.96.064428](https://doi.org/10.1103/PhysRevB.96.064428)

**I. INTRODUCTION**

Spintronics is a multidisciplinary field which involves the study of active manipulation of spin degrees of freedom in solid-state systems [1]. Thermoelectricity concerns the ability of a given material to produce voltage when a temperature gradient is present, thus converting thermal energy to electric energy [2]. The emerging research field of spin caloritronics may be regarded as an interconnection of spintronics and thermoelectricity. One of the well-established phenomena of spin caloritronics is the spin Seebeck effect (SSE) discovered in 2008 by Uchida *et al.* [3]. The SSE is a combination of two phenomena: the generation of a spin current by a temperature gradient applied across a magnetically ordered material, and a conversion of the spin current to electrical current by means of the inverse spin Hall effect (ISHE) [4] in the attached metallic thin layer. A necessary condition for the observation of SSE is that the directions of the spin current, magnetic moments of the magnetic material, and electrical current in the metallic layer have mutually perpendicular components. In analogy with the Seebeck effect, it is possible in the regime of linear response to define a spin Seebeck coefficient  $S_{\text{SSE}} = E_{\text{ISHE}}/\nabla T$ .

In order to avoid additional signals such as a planar or anomalous Nernst effect (ANE) it is more convenient, for the purposes of the SSE, to use magnetic insulators rather than conductors [5–8]. In this respect there are three main types of magnetic insulators having critical temperature of ferrimagnetic ordering  $T_C$  above the room temperature: garnets, spinels, and hexagonal ferrites. Since the spin pumping

is critically limited by the decay of spin waves in the magnetic layer that actively generates the spin flow, so far most of the SSE experiments were based on iron garnets Y<sub>3</sub>Fe<sub>5</sub>O<sub>12</sub> (YIG), as garnets exhibit one of the lowest decays of spin waves with Gilbert damping constant  $\alpha \sim 10^{-3}$ – $10^{-5}$  [9–11].

Magnetic hexagonal ferrites (hexaferrites) typically have higher Gilbert damping constant  $\alpha \sim 10^{-2}$ – $10^{-3}$  [12,13] than garnets. In this paper we have focused on Y-type hexaferrites, namely, Ba<sub>2</sub>Zn<sub>2</sub>Fe<sub>12</sub>O<sub>22</sub> (Zn2Y) and Ba<sub>2</sub>Co<sub>2</sub>Fe<sub>12</sub>O<sub>22</sub> (Co2Y). Since a positive correlation between SSE and the saturation magnetization has been proposed in Ref. [14], their advantage of higher mass magnetizations at room temperature being 42 emu/g for Zn2Y and 34 emu/g for Co2Y [15], compared to 27.6 emu/g of yttrium ferrite garnet [16], makes these robust magnetic insulators highly interesting. Moreover, taking into account their lower thermal conductivity compared to Y<sub>3</sub>Fe<sub>5</sub>O<sub>12</sub> resulting in a higher-temperature gradient for the same heat flow and as a consequence higher magnetic entropy flow, hexaferrites are worth studying as potential materials for the spin current generation in the SSE.

Contrary to the three-dimensional character of the garnet crystal structure, the crystal structure of Y hexaferrites is two dimensional and belongs to the trigonal space group  $R\bar{3}m$  composed of alternating stacks of S (spinel Me<sub>2</sub>Fe<sub>4</sub>O<sub>8</sub>, Me = Zn or Co in our case) and T (Ba<sub>2</sub>Fe<sub>8</sub>O<sub>14</sub>) blocks along the hexagonal *c* axis. The magnetic configuration reflecting the structural aspects leads to ferrimagnetic order; the uncompensated magnetic moment lying in the *ab* plane originates from dominating majority spins in octahedral 3a, 3b, and 18*h* sites and minority spins in tetrahedral 6*c*<sub>T</sub> and 6*c*<sub>S</sub> and octahedral 6*c* sites, respectively (see Fig. 1).

\*Corresponding author: knizek@fzu.cz

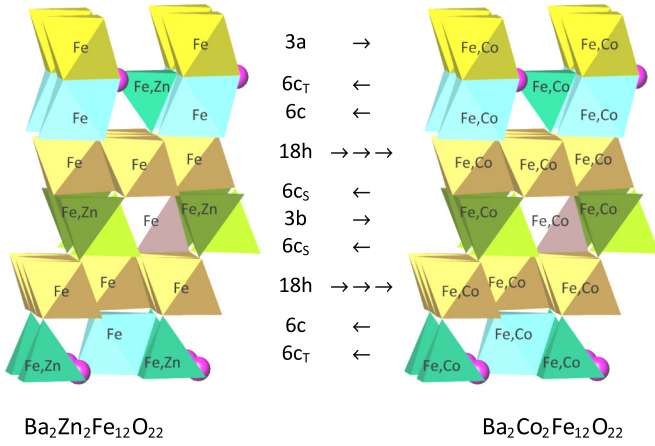


FIG. 1. One formula unit of  $\text{Ba}_2\text{Zn}_2\text{Fe}_{12}\text{O}_{22}$  (left) and  $\text{Ba}_2\text{Co}_2\text{Fe}_{12}\text{O}_{22}$  (right) structures. Shown are Fe, Co, and Zn polyhedra and their mixed occupations, Ba cations (magenta bullets), corresponding Wyckoff positions, and arrows indicating spin direction of the collinear ferrimagnetic structure.

Magnetocrystalline anisotropy, observed in all hexagonal ferrites, means that induced magnetization has a preferred orientation within the crystal structure, either with an easy axis of magnetization in the  $c$  direction or with an easy plane of magnetization perpendicular to the  $c$  direction, the latter being the case of the selected Y hexaferrites. Owing to their direction of easy growth lying in the  $ab$  plane, hexaferrites inherently tend to crystallize with their  $c$  axis perpendicular to the substrate surface when deposited as thin films. Since the magnetization vector in the SSE element should lie parallel to the film surface, the hexaferrites with an easy plane of magnetization are thus very suitable for the SSE experiment.

As concerns the choice of the two systems the principal difference between Zn2Y and Co2Y comes from different site preferences and magnetic properties of  $\text{Zn}^{2+}$  and  $\text{Co}^{2+}$ . The nonmagnetic  $\text{Zn}^{2+}$  ion ( $d^{10}$ ) occupies preferentially the tetrahedral sites in the hexaferrite structure. Since both  $\text{Fe}^{3+}$  in tetrahedral sites (see Fig. 1) have the minor-spin orientation, the substitution of  $\text{Zn}^{2+}$  maximizes the overall magnetic moment and the saturation magnetization  $18.4 \mu_B$  at low temperature reaches more than 90% of theoretical limit  $\approx 20 \mu_B$  given by  $5 \mu_B$  per  $\text{Fe}^{3+}$ . The magnetic  $\text{Co}^{2+}$  ion is in the high-spin state ( $t_{2g}^5 e_g^2$ ) and substitutes  $\text{Fe}^{3+}$  with both major- and minor-spin orientations without evident preferential occupancy [17]. The irregular Co substitution results in partial magnetic disorder and lower saturation magnetization than in Zn2Y; the typical value is around  $10 \mu_B$ . On the other hand, since the critical temperature of ferrimagnetic ordering  $T_C \sim 340^\circ\text{C}$  of Co2Y is higher than  $T_C \sim 130^\circ\text{C}$  of Zn2Y, which reflects the antiferromagnetic (AFM) interactions between  $\text{Fe}^{3+}$  and  $\text{Co}^{2+}$ , the magnetic moment at room temperature around  $8.6 \mu_B$  is not so different from that of Zn2Y (see, e.g., the review paper [15]).

The SSE in a Y-hexaferrite system was recently studied for the Zn2Y phase partially substituted at the Ba site with stoichiometry  $\text{Ba}_{2-x}\text{Sr}_x\text{Zn}_2\text{Fe}_{12}\text{O}_{22}$  ( $x = 1.5$ ) [18]. Most interestingly it was observed that the magnitude of the SSE is proportional to bulk magnetization and is insensitive to the

successive magnetic transitions among various helimagnetic and ferrimagnetic phases, that are stabilized when temperature is lowered. Further, the M-type hexaferrite  $\text{BaFe}_{12}\text{O}_{19}$  was studied in Ref. [13], and since the M-type hexaferrite has strong anisotropy with an easy axis of magnetization in the  $c$  direction a proper substrate and deposition procedure must be selected in order to grow the thin films with the  $c$  axis oriented parallel to the surface of the layer as demanded by the nature of the longitudinal SSE. The advantage of the M type is its high coercive field, which makes the resulting SSE element self-biased, thus producing a SSE signal even without the presence of a magnetic field.

The SSE was also studied in  $\text{Fe}_3\text{O}_4$  with the spinel structure, which may be considered as the simplest structural basis of hexagonal ferrites [19,20], including partially substituted spinels  $(\text{Mn,Zn})\text{Fe}_2\text{O}_4$  and  $\text{NiFe}_2\text{O}_4$  [21,22]. In this respect a large coercive field and high saturation magnetization makes  $\text{Fe}_3\text{O}_4$  promising magnetic material for the investigation of self-biased SSE elements.

The aim of this paper was an investigation of the SSE in two hexagonal ferrites of Y-type  $\text{Ba}_2\text{Zn}_2\text{Fe}_{12}\text{O}_{22}$  and  $\text{Ba}_2\text{Co}_2\text{Fe}_{12}\text{O}_{22}$ , where  $\text{Fe}^{3+}$  is substituted by either the nonmagnetic  $\text{Zn}^{2+}$  or magnetic  $\text{Co}^{2+}$  ion, including the SSE temperature dependence. In order to obtain values comparable with iron garnet  $\text{Y}_3\text{Fe}_5\text{O}_{12}$ , as a currently standard material for SSE, we have calculated the SSE taking into account the heat flow and thermal gradient through the sample thin layer. Concerning this point we note the fact that current research describes the SSE using a typical quantity of the spin Seebeck coefficient in units  $\mu\text{V}/\text{K}$ , which is in conventional thermoelectric materials used for evaluating the effectiveness of the process. However, in most of the experimental setups the temperature sensors measuring the temperature difference  $\Delta T$  are attached to the SSE measurement cell itself. This implies that  $\Delta T$  describes not merely the thermal characteristics of the studied layered material but the whole measurement cell instead, which makes the quantity in units of  $\mu\text{V}/\text{K}$  physically irrelevant to the SSE itself. This issue was studied in detail in Refs. [23,24]. Most importantly the authors pointed out that when using the setup dependent  $\Delta T$  as the independent variable the determined SSE can be hardly comparable between laboratories. In order to solve this problem, the authors designed a measurement system with precise measurement of the heat flow through the sample and proposed using heat flow or thermal gradient at the sample as the independent variable. We have followed this approach and we have shown that the total temperature difference  $\Delta T$  is not appropriate to quantify the temperature dependence of the SSE coefficient of a studied material, namely, as a result of the temperature evolution of thermal conductivity of the whole experimental setup, which may significantly differ from that of the sample itself.

## II. EXPERIMENTAL

Thin films of Zn2Y and Co2Y were prepared by spin-coating technique on (111)-oriented, epitaxially polished  $\text{SrTiO}_3$  single crystals (MaTecK GmbH, Germany) with metal-organic precursor solutions. Commercial 2-ethylhexanoates  $\text{Me}(\text{CH}_3(\text{CH}_2)_3\text{CH}(\text{C}_2\text{H}_5)\text{COO})_n$  ( $n = 2$  for  $\text{Me} = \text{Ba, Co, Zn}$ ;  $n = 3$  for  $\text{Me} = \text{Fe}$ ; abcr GmbH, Germany) were used

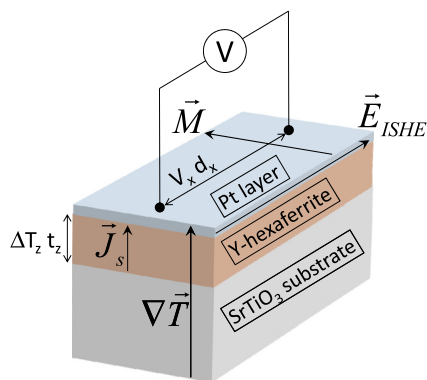


FIG. 2. Schema of the longitudinal experimental configurations. Directions of spin current ( $\vec{J}_s$ ), temperature gradient ( $\nabla\vec{T}$ ), magnetization ( $\vec{M}$ ), and electrical field resulted from inverse spin Hall effect ( $\vec{E}_{ISHE}$ ), are shown. The meaning of parameters  $V_x$ ,  $t_z$ ,  $d_x$ , and  $\Delta T_z$  used in Eq. (4) is also indicated.

as precursors. Calculated amounts of metal precursors were dissolved in isobutanol, mixed, and heated for several hours at 80 °C to accomplish homogenization. Subsequently a suitable amount of 2,2-diethanolamine (DEA) used as a modifier was added. The modifier to alkaline-earth-metal molar ratio was  $n(\text{DEA})/n(\text{alkaline-earth metal}) = 2$ . Prior to the deposition the stock solutions were usually diluted with isobutanol to obtain films of desired thickness. All reactions and handling were done under dry nitrogen atmosphere to prevent reaction with air humidity and preliminary formation of alkaline-earth carbonates in solutions. Single crystals of SrTiO<sub>3</sub> were washed in acetone combined with sonication and then annealed at 1200 °C in air for 24 h to heal up the surface damage caused during polish treatment. Prior to the deposition they were treated with plasma (Zepto Plasma cleaner, Diener Electronic, Germany). After the drying at 110 °C for several minutes and pyrolysis of gel films at 300 °C for 5 min, crystallization annealing was done at 1000 °C for 5 min in a conventional tube furnace under open air atmosphere. The deposition-annealing cycle was repeated ten times to obtain the desired film with approximately 150–350 nm of thickness. Final annealing was done in a tube furnace under open air atmosphere at 1050 °C for 5 min (Zn<sub>2</sub>Y) or 1000 °C for 60 min (Co<sub>2</sub>Y).

The SSE was measured using a home-made apparatus. A longitudinal configuration was used, in which the directions of the spin current, magnetic moments, and electrical current are mutually perpendicular (see Fig. 2). An AlN plate, as a thermally conducting and electrically insulating material, was used to separate the heater and the sample in order to uniformly spread the heat flow over the sample area. The application of an accurate and repeatable compressive load using a microtorque wrench for sample mounting ensured the minimization of interfacial thermal barriers between individual parts of the measurement cell which was further complemented by using appropriate greases (Apiezon type N, Dow Corning Varnish). To ensure the majority of the heat flow being propagated through the sample, a mounting part was designed to have low thermal conductivity with stable thermal dependency, using a teflon sheet fastened by nylon screws. The small voltage was measured using a Keithley 2182A nanovoltmeter and the experiment was fully automated.

The width of the measured sample was set to 2 mm, the length was set to 7 mm, and the electric contact distance (on the Pt layer) was 5 mm. Thickness of the Zn<sub>2</sub>Y-hexaferrite layers varied between 300 and 350 nm, and the thickness for Co<sub>2</sub>Y-hexaferrite layers ranged between 150 and 300 nm. The Pt layer converting spin current to voltage was deposited using a K550X Quorum Technologies sputter coater. The thickness of the Pt layer was determined by an internal film thickness monitor set to ~8 nm. The electric resistance of the Pt layer measured by a two-point technique varied for respective samples in the series within the range 350–650 Ω at room temperature, and linearly decreased by 10–15% down to 5 K. By comparison with the resistivity of Pt films with variable thickness determined in Ref. [25], we estimate the minimum effective thickness of our Pt films as 2–3 nm. The resistance of the Y-hexaferrite thin layer itself was more than 1 GΩ over the whole temperature range. Therefore, as anticipated, the contribution from the ANE to the measured signal can be considered as negligible due to the lack of free charge carriers in the Y hexaferrite.

The magnetic response of the samples was measured within the range of magnetic field from –25 to 25 kOe at room temperature using a superconducting quantum interference device magnetometer (MPMSXL, Quantum Design).

The phase purity and degree of preferred orientation of the thin films was checked by x-ray diffraction (XRD) over the angular range  $2\theta$  from 10 to 100° using the x-ray powder diffractometer Bruker D8 Advance (CuK $\alpha_{1,2}$  radiation, secondary graphite monochromator). An atomic force microscopy (Explorer, Thermomicroscopes, USA) was used to evaluate surface microstructure of the thin films.

### III. RESULTS AND DISCUSSION

The x-ray diffraction confirmed single phase purity of the thin film and  $c$ -axis preferred orientation, quantified by the full width at half maximum of the rocking curve as 0.45° for Zn<sub>2</sub>Y and 0.58° for Co<sub>2</sub>Y (see Fig. 3). The  $c$ -lattice parameters 43.567(7) Å for Zn<sub>2</sub>Y and 43.500(9) Å for Co<sub>2</sub>Y, calculated

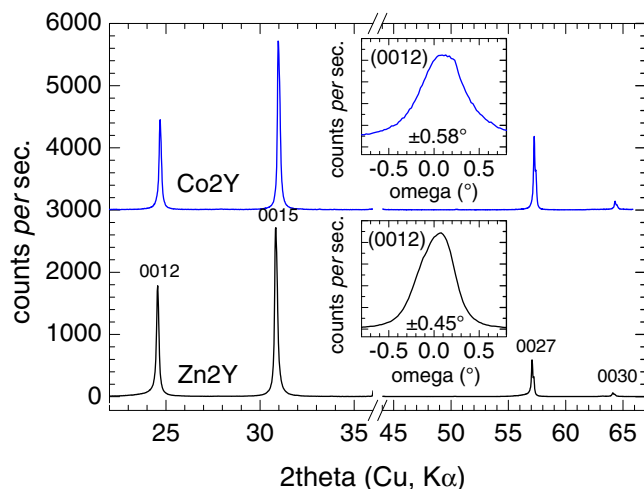


FIG. 3. X-ray diffraction of the Zn<sub>2</sub>Y (black line) and Co<sub>2</sub>Y (blue line) thin film. The insets show rocking-curve measurements. The diffraction peak (111) of the SrTiO<sub>3</sub> substrate is skipped.

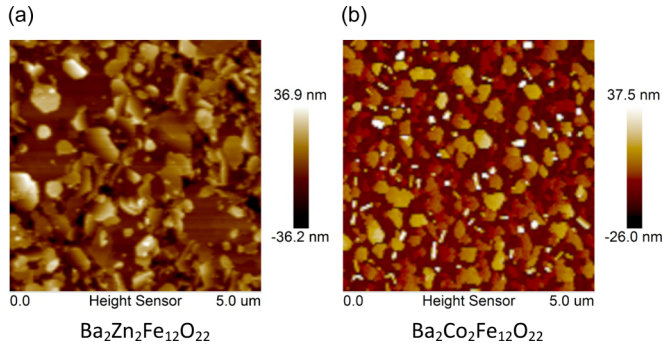


FIG. 4. AFM images of surface topography of (a) Zn2Y (calculated roughness rms = 12 nm) and (b) Co2Y (rms = 8 nm).

using  $\cos \theta / \tan \theta$  extrapolation to correct a possible off-center position of the film during XRD measurement, are in good agreement with literature values [26].

Figure 4 shows AFM images of surface topography of Zn2Y and Co2Y. Platelets with hexagonal shape can be identified in both images with similar shape and size. Calculated roughness (rms) values are around 8–12 nm.

The magnetic properties of the Y-hexaferrite thin layers were characterized by magnetization curves measured at room temperature. The magnetic moment of Zn2Y determined from the saturated value of magnetization in parallel orientation is  $\simeq 11 \mu_B$  (see the upper panel of Fig. 5), which is comparable with the expected value [15]. The measurement confirms

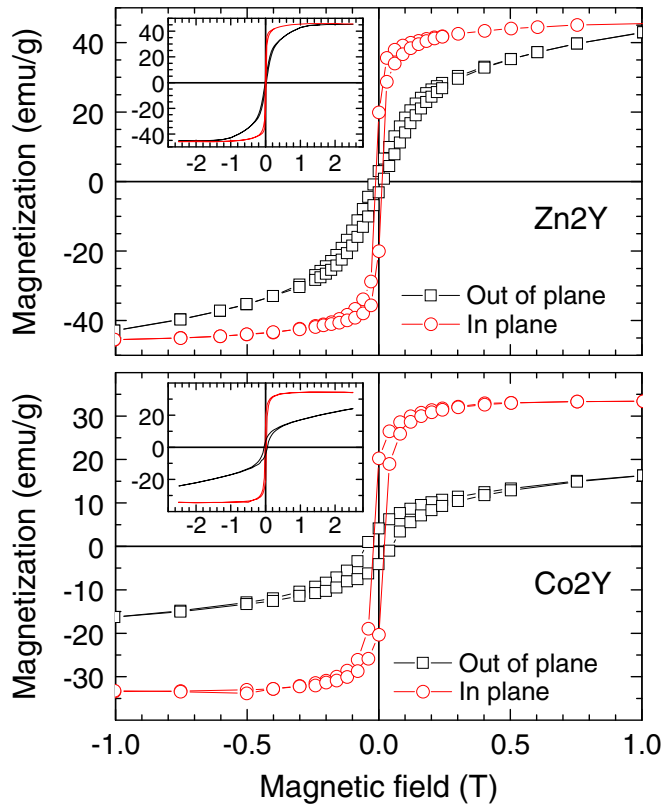


FIG. 5. In-plane and out-of-plane magnetization in dependence on magnetic field at 300 K for Zn2Y (upper panel) and Co2Y (lower panel).

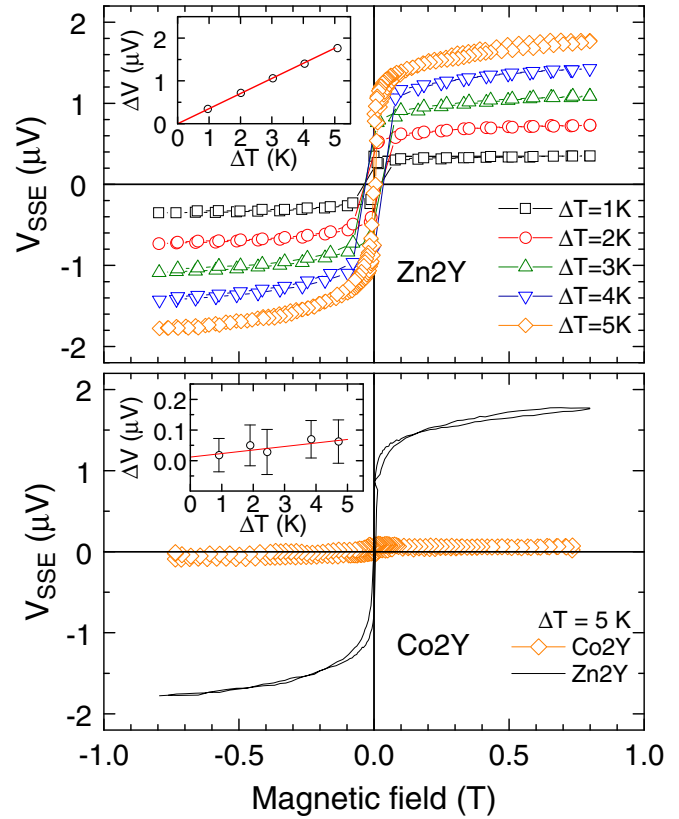


FIG. 6. Upper panel: SSE voltage dependence on magnetic field for Zn2Y at 300 K under various temperature differences  $\Delta T$ . Lower panel: SSE voltage of Co2Y in comparison with Zn2Y.

that Zn2Y is a soft magnet with negligible hysteresis. The saturation in the orientation parallel to the thin layer is attained already at low field, whereas the saturation in the out-of-plane orientation, i.e., along the  $c$  direction, is achieved at higher field above 1 T, in agreement with the  $ab$  easy-plane orientation.

The magnetic moment of Co2Y at room temperature determined from the saturated value of magnetization in parallel orientation is  $10 \mu_B/\text{f.u.}$  (see the lower panel of Fig. 5). This value is slightly higher than the expected one [15], presumably due to a relatively higher structural preference of Co for minor-spin sites in the case of our thin films as the expected value was derived for bulk samples. The difference between the magnetic saturation in parallel and perpendicular orientation is larger in agreement with higher magnetocrystalline anisotropy of Co2Y compared to Zn2Y.

The spin Seebeck signal for various temperature differences  $\Delta T$  of Zn2Y at room temperature is displayed in the upper panel of Fig. 6. The measured voltage is positive in positive external magnetic field, which is in agreement with the positive spin Hall angle of Pt [27], and the voltage changes sign when switching the polarity of the magnetic field. The variation of the spin Seebeck signal with external magnetic field is highly reminiscent of the magnetization data in parallel orientation, i.e., it has the same shape with negligible hysteresis. Furthermore the spin Seebeck voltage data clearly show linear dependence on temperature difference  $\Delta T$ .

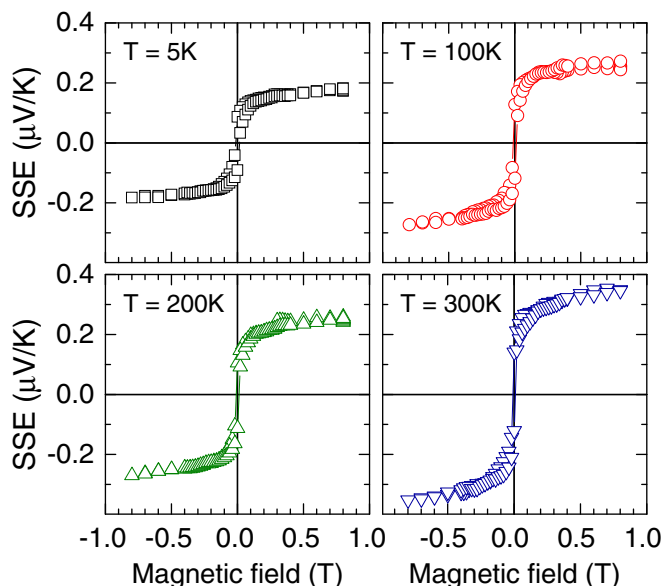


FIG. 7. SSE normalized to the total temperature difference  $\Delta T$  at selected temperatures.

Despite the similar magnetic properties within the *ab* plane of Zn2Y and Co2Y, no SSE signal, which could be distinguished from the experimental noise level and thermal drift of the signal, was detected for any of several investigated Co2Y samples, as depicted for the selected sample in the lower panel of Fig. 6 in comparison with Zn2Y. No distinguishable SSE signal was observed, either, during measurement at low temperature down to 5 K. To explain this essentially different behavior of Zn2Y and Co2Y hexaferrites, we must consider the difference in the cation distributions of the transition-metal cations over the structure (see the Introduction and Fig. 1). Since the  $\text{Zn}^{2+}$  ion is nonmagnetic, the layer of  $\text{Ba}_2\text{Zn}_2\text{Fe}_{12}\text{O}_{22}$  only contains one type of magnetic ion with the Zn cation preferentially substituting  $\text{Fe}^{3+}$  in two tetrahedral sites with the same direction of spin polarization. As a consequence the total spin polarization of the unit cell does not significantly fluctuate across the material. In distinction, the  $\text{Ba}_2\text{Co}_2\text{Fe}_{12}\text{O}_{22}$  contains two types of magnetic ions, i.e.,  $\text{Co}^{2+}$  in addition to  $\text{Fe}^{3+}$ . Cobalt ions substitute  $\text{Fe}^{3+}$  in all positions without strong preference for a particular site where Fe ions may have both major- and minor-spin orientation. Therefore we propose that this random distribution of  $\text{Co}^{2+}$  over various sites with both spin polarizations interferes with the long-range magnetic ordering across the material, diminishes the spin-wave propagation and the spin currents, and results in a strong suppression of the SSE signal.

As measurement at 300 K on Zn2Y layers insinuated notable SSE effect the temperature evolution of SSE loops of Zn2Y was measured at several temperatures down to 5 K with the output power of the heater fixed for all temperatures (see the measurements at selected temperatures 5, 100, 200, and 300 K in Fig. 7). The character of the loops is not changed with lowering temperature; only the magnitude of the SSE signal varies.

To investigate the temperature dependence of the SSE signal of Zn2Y below room temperature in more detail, we

have performed SSE measurement down to 30 K with 10-K steps. In this case, similarly as in the previous experiment, the output power of the heater was also kept constant during this measurement. The value of the SSE voltage was determined by switching the magnetic field to  $\pm 0.4$  T at each temperature and calculating the difference:

$$V_{\text{SSE}} = \frac{V_{+0.4\text{T}} - V_{-0.4\text{T}}}{2}. \quad (1)$$

In order to grasp quantitatively the effectiveness of the generation of the SSE using Zn2Y the resulting temperature dependence is displayed in Fig. 8 in three ways. In the upper part of the figure, Fig. 8(a), the SSE signal is normalized by the total temperature difference  $\Delta T$  determined over the whole measuring cell. The temperature evolution of  $\Delta T$  (shown in the inset) revealed that  $\Delta T$  increased several times when absolute temperature was lowered to 30 K. Since the output power of the heater was kept constant, this increase should be related to a decrease of the thermal conductance of the materials and barriers between the temperatures probes.

In order to obtain a setup independent SSE, the measured voltage  $V_{\text{SSE}}$  should be normalized by the temperature difference at the magnetic material itself  $\Delta T_z$  measured along the thickness of the material  $t_z$  (see Fig. 2), as it was proposed in Refs. [23,24]. The quantity  $\Delta T_z$  is practically impossible to measure directly, but it can be calculated using the heat flow  $P$  through the sample (corrected for the heat losses due to radiation), the thermal conductivity of the magnetic material  $\lambda_z$ , and the appropriate size factor  $t_z/A$ , where  $A$  is the heated area of the sample:

$$\Delta T_z = P \frac{t_z}{\lambda_z A}. \quad (2)$$

If the thermal conductivity of the magnetic material is not known, the measured SSE voltage  $V_{\text{SSE}}$  can be normalized by the heat flow through the sample, as this quantity is directly related to  $\Delta T_z$  for a given material:

$$S_{\text{SSE}}^W = \frac{V_{\text{SSE}}}{P} [V/W]. \quad (3)$$

The SSE voltage divided by the heat flow through the sample  $S_{\text{SSE}}^W$  is shown in Fig. 8(b) with corresponding heat flow in the inset.

Nevertheless, in order to extract a quantity comparable not only over different measurement setups but also for different materials (with various thermal conductivity), an expression for the SSE related to the temperature difference over the sample itself  $\Delta T_z$  and the sample dimensions was defined [23,28]:

$$S_{\text{SSE}} = \frac{V_x t_z}{d_x \Delta T_z} [V/K] \quad (4)$$

where  $V_x = V_{\text{SSE}}$  and  $d_x$  is the electric contact distance (see Fig. 2). In order to calculate  $\Delta T_z$  over the whole experimental temperature range, we have measured the temperature dependence of thermal conductivity of the bulk sample  $\text{Ba}_2\text{Zn}_2\text{Fe}_{12}\text{O}_{22}$  synthesized from the precursors used for the thin layer deposition and compacted by isostatic pressing [see Fig. 8(c)].

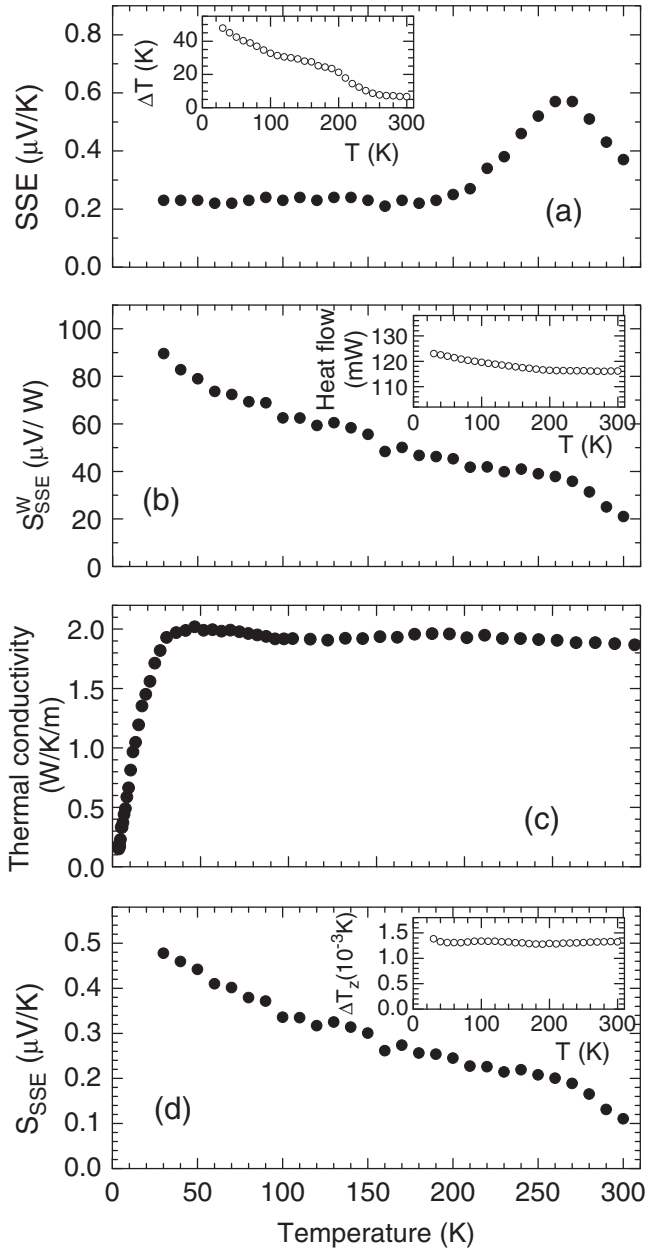


FIG. 8. (a) SSE dependence on temperature for Zn2Y divided by the overall temperature gradient, where the inset shows corresponding temperature difference  $\Delta T$ . (b)  $S_{\text{SSE}}^W$  divided by the heat flow through the sample [see Eq. (3)], where the inset shows corresponding heat flow  $P$ . (c) Thermal conductivity of bulk  $\text{Ba}_2\text{Zn}_2\text{Fe}_{12}\text{O}_{22}$ . (d)  $S_{\text{SSE}}$  divided by the temperature difference at the magnetic material [see Eq. (4)], where the inset shows corresponding temperature difference  $\Delta T_z$ .

With the knowledge of the heat flow and the thermal conductivity of the sample material Zn2Y we were able to calculate  $\Delta T_z$  and consequently  $S_{\text{SSE}}$  according to Eq. (4) [see the temperature dependence in Fig. 8(d); the evolution of  $\Delta T_z$  is displayed in the inset].

The correct normalization of the SSE signal is important not only for comparing among various measurement setups but also for the correct determination of its temperature dependence, as is evident by comparison of various tem-

perature evolutions of the SSE shown in Fig. 8. The SSE related to the total temperature difference  $\Delta T$  [Fig. 8(a)] shows incorrect temperature dependence influenced by the temperature dependence of the total thermal conductivity of the measuring setup. We propose that the correct temperature dependence is determined by relating the SSE to heat flow [Fig. 8(b)] or to temperature difference at the sample  $\Delta T_z$  [Fig. 8(d)]. In this case, the SSE is almost linearly increasing with lowering temperature.

The almost five-factor increase of the SSE at 30 K compared to room temperature can be partially explained by the increased magnetization (almost  $2\times$ ), but the decrease of Gilbert damping factor  $\alpha$  should be of greater influence in this regard. As determined in the study of the temperature dependence of the SSE signal in  $\text{Y}_3\text{Fe}_5\text{O}_{12}$  garnet [29], the effective propagation length of thermally excited magnons  $\xi$  is proportional to  $T^{-1}$ , and since at the same time  $\alpha \sim \xi^{-1}$  [30,31] this means that Gilbert damping factor  $\alpha$ , which is expected to influence essentially the SSE signal, is linearly decreasing with temperature.

In distinction to temperature dependence of the SSE in YIG [29], where a maximum in SSE was observed and explained by the interplay of the increase of magnon effective propagation length and decrease of the total number of thermally excited magnons, we observed monotonous increase down to 30 K. We ascribe this observation to the lower dispersion of acoustic branches in magnon spectra of Y hexaferrite, which makes the influence of increasing total number of thermally excited magnons less important.

Confronting the normalized room-temperature values of Y hexaferrite with YIG garnet, we have determined characteristic parameters: (i) the SSE normalized to heat flow through the sample  $S_{\text{SSE}}^W = 21 \mu\text{V}/\text{W}$  and (ii) SSE calculated according to Eq. (4)  $S_{\text{SSE}} = 0.11 \mu\text{V}/\text{K}$  for Zn2Y. These characteristics evaluated for Y-hexagonal ferrite Zn2Y are somewhat lower in comparison with  $S_{\text{SSE}}^W = 46.6 \mu\text{V}/\text{W}$  and  $S_{\text{SSE}} = 0.28 \mu\text{V}/\text{K}$  determined for  $\text{Y}_3\text{Fe}_5\text{O}_{12}$  [23]. We propose as an origin of this difference the lower Gilbert damping constant  $\alpha$  and/or a higher dispersion of acoustic branches in magnon spectra of  $\text{Y}_3\text{Fe}_5\text{O}_{12}$ . However, the higher roughness of the surface of the Zn2Y layer and different quality of the Pt layer might negatively influence spin mixing conductance at the Zn2Y/Pt interface and spin Hall angle of Pt, respectively, and thus also contribute to reduction of the  $S_{\text{SSE}}$  value of our Zn2Y sample. Nevertheless, we have proved that despite the rather complex magnetic structure of Y hexaferrites they can be used as highly efficient spin sources down to low temperatures.

#### IV. CONCLUSIONS

The longitudinal SSE has been investigated in thin films of two Y-hexagonal ferrites  $\text{Ba}_2\text{Zn}_2\text{Fe}_{12}\text{O}_{22}$  and  $\text{Ba}_2\text{Co}_2\text{Fe}_{12}\text{O}_{22}$  deposited by spin-coating method on the  $\text{SrTiO}_3(111)$  substrate. The significant SSE signal was observed for Zn2Y, whereas no SSE signal distinguishable from the experimental noise level and thermal drift is detected for Co2Y. A plausible explanation for the absence of the SSE signal in Co2Y might be attributed to the presence of two different magnetic ions  $\text{Fe}^{3+}$  and  $\text{Co}^{2+}$ , the random distribution of which interferes

with long-range ordering and critically limits spin-wave propagation. However, further studies are needed to confirm this hypothesis. The magnitude of the spin Seebeck signal of Zn<sub>2</sub>Y normalized to the temperature gradient across the investigated magnetic layer and sample dimensions ( $S_{SSE}$ ) is comparable to the results measured on yttrium iron garnet Y<sub>3</sub>Fe<sub>5</sub>O<sub>12</sub> [23]. Additional normalization to the spin mixing conductance and spin Hall angle might be taken into consideration in order to make the comparison fully relevant. As regards the resistance of the Pt layer, it is not crucial for the present experiments performed under the open-circuit condition (it might only influence the precision of the nanovolt signal detection), but it becomes important for the whole SSE device performance, since it determines the internal resistance of the SSE device, as it was shown by measuring current-voltage-power characteristics in Ref. [32]. The  $S_{SSE}$  of Zn<sub>2</sub>Y monotonously increases with decreasing

temperature down to 30 K, which is likely a synergic result of the simultaneous increase of the magnetization and magnon effective propagation length.

#### ACKNOWLEDGMENTS

This work was supported by Project No. 14-18392S of the Czech Science Foundation, Grant No. SGS16/245/OHK4/3T/14 of the Czech Technical University in Prague, the Spanish Ministry of Economy and Competitiveness (Grant No. MAT2014-51982-C-R, including FEDER), and the Aragon Regional government (E26). The authors acknowledge the Advanced Microscopy Laboratory-INA, University of Zaragoza for offering access to their instruments. The work was also supported by Thermo-Spintronic FP7-PEOPLE-2011-Marie Curie, CIG Project No. 304043, and SPICOLST project H2020-MSCA-2016 Grant No. 734187.

- 
- [1] Y. Xu, D. D. Awschalom, and J. Nitta, *Handbook of Spintronics* (Springer, New York, 2015).
- [2] D. M. Rowe, *Thermoelectrics Handbook: Macro to Nano* (Taylor & Francis, London, 2005).
- [3] K. Uchida, S. Takahashi, K. Harii, J. Ieda, W. Koshibae, K. Ando, S. Maekawa, and E. Saitoh, Observation of the spin Seebeck effect, *Nature (London)* **455**, 778 (2008).
- [4] E. Saitoh, M. Ueda, H. Miyajima, and G. Tatara, Conversion of spin current into charge current at room temperature: Inverse spin-Hall effect, *Appl. Phys. Lett.* **88**, 182509 (2006).
- [5] K. Uchida, J. Xiao, H. Adachi, J. Ohe, S. Takahashi, J. Ieda, T. Ota, Y. Kajiwara, H. Umezawa, H. Kawai, G. E. W. Bauer, S. Maekawa, and E. Saitoh, Spin Seebeck insulator, *Nat. Mater.* **9**, 894 (2010).
- [6] S. Y. Huang, W. G. Wang, S. F. Lee, J. Kwo, and C. L. Chien, Intrinsic Spin-Dependent Thermal Transport, *Phys. Rev. Lett.* **107**, 216604 (2011).
- [7] A. D. Avery, M. R. Pufall, and B. L. Zink, Observation of the Planar Nernst Effect in Permalloy and Nickel Thin Films with In-Plane Thermal Gradients, *Phys. Rev. Lett.* **109**, 196602 (2012).
- [8] M. Schmid, S. Srichandan, D. Meier, T. Kuschel, J. M. Schmalhorst, M. Vogel, G. Reiss, C. Strunk, and C. H. Back, Transverse Spin Seebeck Effect versus Anomalous and Planar Nernst Effects in Permalloy Thin Films, *Phys. Rev. Lett.* **111**, 187201 (2013).
- [9] H. Adachi, J. I. Ohe, S. Takahashi, and S. Maekawa, Linear-response theory of spin Seebeck effect in ferromagnetic insulators, *Phys. Rev. B* **83**, 094410 (2011).
- [10] M. Schreier, A. Kamra, M. Weiler, J. Xiao, G. E. W. Bauer, R. Gross, and S. T. B. Goennenwein, Magnon, phonon, and electron temperature profiles and the spin Seebeck effect in magnetic insulator/normal metal hybrid structures, *Phys. Rev. B* **88**, 094410 (2013).
- [11] S. Hoffman, K. Sato, and Y. Tserkovnyak, Landau-Lifshitz theory of the longitudinal spin Seebeck effect, *Phys. Rev. B* **88**, 064408 (2013).
- [12] I. Harward, Y. Nie, D. Chen, J. Baptist, J. M. Shaw, E. Jakubisová-Lišková, S. Višňovský, P. Šíroky, M. Lesňák, J. Pištora, and Z. Celinski, Physical properties of Al doped hexagonal ferrite thin films, *J. Appl. Phys.* **113**, 043903 (2013).
- [13] P. Li, D. Ellsworth, H. C. Chang, P. Janantha, D. Richardson, F. Shah, P. Phillips, T. Vijayarathy, and M. Z. Wu, Generation of pure spin currents via spin Seebeck effect in self-biased hexagonal ferrite thin films, *Appl. Phys. Lett.* **105**, 242412 (2014).
- [14] K. Uchida, T. Nonaka, T. Kikkawa, Y. Kajiwara, and E. Saitoh, Longitudinal spin Seebeck effect in various garnet ferrites, *Phys. Rev. B* **87**, 104412 (2013).
- [15] R. C. Pullar, Hexagonal ferrites: A review of the synthesis, properties and applications of hexaferrite ceramics, *Prog. Mater. Sci.* **57**, 1191 (2012).
- [16] NIST Standard Reference Material 2853, Magnetic Moment Standard: Yttrium Iron Garnet Sphere (2002).
- [17] H.-S. Shin, S. G. Lee, and S.-J. Kwon, Properties of hexaferrite Co<sub>2</sub>Y(Ba<sub>2</sub>Co<sub>2</sub>Fe<sub>12</sub>O<sub>22</sub>) prepared by coprecipitation method, *J. Korean Ceram. Soc.* **29**, 195 (1992).
- [18] R. Takagi, Y. Tokunaga, T. Ideue, Y. Taguchi, Y. Tokura, and S. Seki, Thermal generation of spin current in a multiferroic helimagnet, *APL Mater.* **4**, 032502 (2016).
- [19] A. J. Caruana, M. D. Cropper, J. Zipfel, Z. X. Zhou, G. D. West, and K. Morrison, Demonstration of polycrystalline thin film coatings on glass for spin Seebeck energy harvesting, *Phys. Status Solidi: Rapid Res. Lett.* **10**, 613 (2016).
- [20] R. Ramos, A. Anadon, I. Lucas, K. Uchida, P. A. Algarabel, L. Morellon, M. H. Aguirre, E. Saitoh, and M. R. Ibarra, Thermoelectric performance of spin Seebeck effect in Fe<sub>3</sub>O<sub>4</sub>/Pt-based thin film heterostructures, *APL Mater.* **4**, 104802 (2016).
- [21] K. Uchida, T. Nonaka, T. Ota, and E. Saitoh, Longitudinal spin-Seebeck effect in sintered polycrystalline (Mn, Zn)Fe<sub>2</sub>O<sub>4</sub>, *Appl. Phys. Lett.* **97**, 262504 (2010).
- [22] D. Meier, T. Kuschel, L. Shen, A. Gupta, T. Kikkawa, K. Uchida, E. Saitoh, J. M. Schmalhorst, and G. Reiss, Thermally driven spin and charge currents in thin NiFe<sub>2</sub>O<sub>4</sub>/Pt films, *Phys. Rev. B* **87**, 054421 (2013).
- [23] A. Sola, M. Kuepferling, V. Basso, M. Pasquale, T. Kikkawa, K. Uchida, and E. Saitoh, Evaluation of thermal gradients in longitudinal spin Seebeck effect measurements, *J. Appl. Phys.* **117**, 17C510 (2015).

- [24] A. Sola, P. Bougiatioti, M. Kuepferling, D. Meier, G. Reiss, M. Pasquale, T. Kuschel, and V. Basso, Longitudinal spin Seebeck coefficient: Heat flux vs. temperature difference method, *Sci. Rep.* **7**, 46752 (2017).
- [25] J. S. Agustsson, U. B. Arnalds, A. S. Ingason, K. B. Gylfason, K. Johnsen, S. Olafsson, and J. T. Gudmundsson, Growth, coalescence, and electrical resistivity of thin Pt films grown by dc magnetron sputtering on SiO<sub>2</sub>, *Appl. Surf. Sci.* **254**, 7356 (2008).
- [26] H. S. Shin and S.-J. Kwon, X-ray powder diffraction patterns of two Y-type hexagonal ferrites, *Powder Diffr.* **8**, 98 (1993).
- [27] M. Schreier, G. E. W. Bauer, V. I. Vasyuchka, J. Flipse, K. Uchida, J. Lotze, V. Lauer, A. V. Chumak, A. A. Serga, S. Daimon, T. Kikkawa, E. Saitoh, B. J. van Wees, B. Hillebrands, R. Gross, and S. T. B. Goennenwein, Sign of inverse spin Hall voltages generated by ferromagnetic resonance and temperature gradients in yttrium iron garnet platinum bilayers, *J. Phys. D* **48**, 025001 (2015).
- [28] C. M. Jaworski, J. Yang, S. Mack, D. D. Awschalom, J. P. Heremans, and R. C. Myers, Observation of the spin-Seebeck effect in a ferromagnetic semiconductor, *Nat. Mater.* **9**, 898 (2010).
- [29] E. J. Guo, J. Cramer, A. Kehlberger, C. A. Ferguson, D. A. MacLaren, G. Jakob, and M. Klaui, Influence of Thickness and Interface on the Low-Temperature Enhancement of the Spin Seebeck Effect in YIG Films, *Phys. Rev. X* **6**, 031012 (2016).
- [30] U. Ritzmann, D. Hinzke, and U. Nowak, Propagation of thermally induced magnonic spin currents, *Phys. Rev. B* **89**, 024409 (2014).
- [31] U. Ritzmann, D. Hinzke, A. Kehlberger, E. J. Guo, M. Klaui, and U. Nowak, Magnetic field control of the spin Seebeck effect, *Phys. Rev. B* **92**, 174411 (2015).
- [32] K. Uchida, M. Ishida, T. Kikkawa, A. Kirihara, T. Murakami, and E. Saitoh, Longitudinal spin Seebeck effect: From fundamentals to applications, *J. Phys.: Condens. Matter* **26**, 343202 (2014).